BEHAVIOUR OF SINGLE CRYSTAL SUPERALLOYS UNDER CYCLIC LOADING AT HIGH TEMPERATURES

Holger Frenz, Joachim Kinder, Hellmuth Klingelhöffer and Pedro D. Portella
Federal Institute for Materials Research and Testing (BAM)
Unter den Eichen 87, D-12205 Berlin, Germany

Abstract

The LCF-behaviour of two single crystal superalloys developed as blade materials for the use in aircraft engines, *viz.* SRR99 and CMSX-6, was investigated at 980°C. Special attention was given to the influence of hold periods at either the maximum (tension phase) or the minimum (compression phase) strain level. The introduction of a hold period in the compression phase led for both alloys to a pronounced reduction of the cycle number for crack initiation, N_A, when compared with the values obtained at the same total strain range, $\Delta\epsilon_t$, without hold periods. This reduction was accentuated by reducing $\Delta\epsilon_t$. On the other hand, the influence of a hold period in the tension phase on N_A was much less pronounced. The evolution of the γ/γ'-microstructure and the fracture mechanisms characteristic for the different loading conditions were investigated using mainly SEM. First results concerning the LCF-behaviour at 950°C of SC 16, a single crystal superalloy developed for the use in land-based industrial gas turbines, are also presented.

Introduction

Under normal service conditions, gas turbine blades are subjected to very complex stress-strain-temperature loading cycles in a non-inert environment. The identification of the predominant damage mechanisms requires careful testing under controlled conditions. In this sense, the introduction of more realistic thermal-mechanical fatigue testing contributes to a better understanding of the material behaviour in real blades (1). However, the high costs of such complex tests and the difficulties in interpretating their results keep a living interest in isothermal low-cycle fatigue testing (1,2).

In this work we present some results concerning the LCF-behaviour of single crystal nickel-base superalloys with and without hold periods. Due to their relatively simple microstructure, single crystal superalloys permit a more detailed investigation of the microstructural modifications as well as of the fracture mechanisms and how they depend on cyclic loading.

Experimental details

The specimens were cast by Thyssen Guß AG in Bochum, Germany, using a high gradient DS/SX-furnace (3). Six specimens were produced in each run by using helix selectors. The chemical composition of each master charge as determined by X-ray spectrometry or atomic absorption spectrometry is given in Table I. The heat treatment consisted of a multi-step solution treatment followed by a two-step ageing treatment according to the standard specification of each alloy.

The resulting microstructure, Figure 1, consisted of a monomodal distribution of cuboidal γ'-particles for SRR99 and CMSX-6 and a bimodal distribution of fine spherical and larger cuboidal γ'-particles for SC 16. Table II summarizes the microstructural parameters of each batch as determined either by point analysis with a light microscope or by area analysis of SEM pictures using a computer assisted system. Metallographic specimens were conventionally prepared paying attention to the orientation of the specimen surface and by using etchant solutions which preferentially etched the γ'-phase. Both SE- and BSE-modes of SEM were used to observe the γ/γ'-microstructure. The problems associated with the determination of the γ' volume fraction based on the measurement of the area fraction in etched metallographic

Table I Chemical composition of the master charges (Mass fractions in %)

Alloy	Ni	Cr	Al	Ti	Mo	W	Co	Ta	others
SRR99	66.05	8.53	5.57	2.22	0.03	9.53	5.03	2.85	0.18
CMSX-6	70.48	9.76	4.78	4.68	3.00	0.03	5.02	2.08	0.17
SC 16	70.93	16.37	3.46	3.50	2.84	0.09	0.05	3.60	0.16

Superalloys 1996
Edited by R. D. Kissinger, D. J. Deye, D. L. Anton,
A. D. Cetel, M. V. Nathal, T. M. Pollock, and D. A. Woodford
The Minerals, Metals & Materials Society, 1996

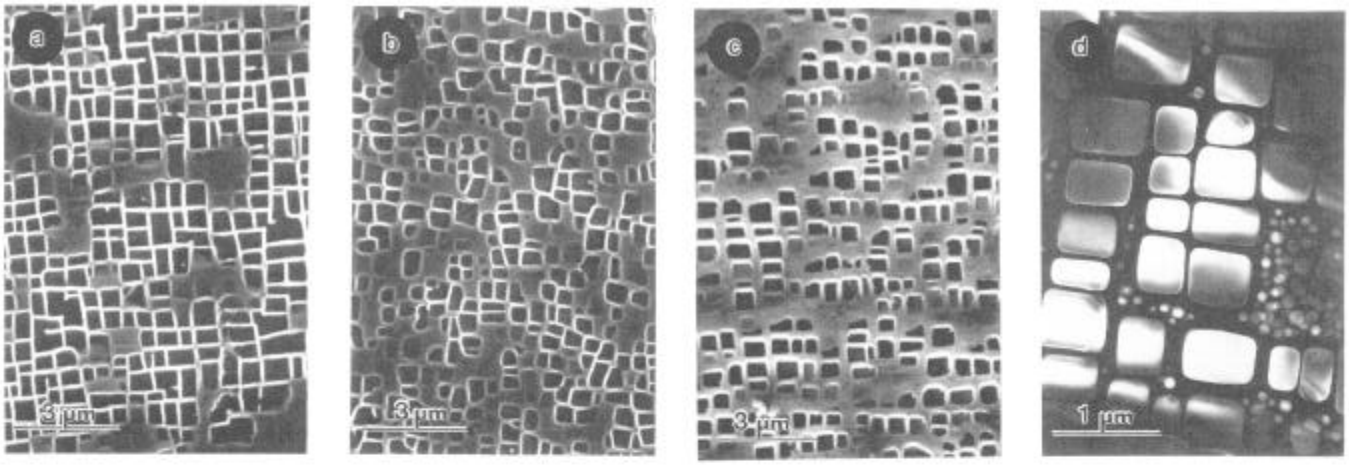

Figure 1: Initial microstructure of: a) SRR99 (SEM); b) CMSX-6 (SEM); c) SC 16 (SEM); d) SC 16 (TEM)

Table II Microstructural parameters of the specimens after the standard heat treatment

Alloy	γ'-phase			porosity		γ/γ'-eutetics
	V_V in %	edge length [1] in µm	diameter [2] in µm	V_V in %	maximal feret in µm	V_V in %
SRR99	60	0.52	-	< 0.5	15	< 0.1
CMSX-6	62	0.57	-	< 0.5	10	2
SC 16	36	0.45	0.08	< 1.0	30	nearly 0

[1] cuboidal particles
[2] spheroidal particles

specimens at the SEM were discussed elsewhere (4,5). The orientation of the specimens was determined by Thyssen Guß using a SCAMP system (6). The angle between the specimen symmetry axis and the [001] direction, χ, varied between 2° and 8° with a median of 5°. The specimens used in the mechanical tests had a total length of 115 mm and a gauge length of 26 mm with 9 mm diameter. Their final shape was given by circumferential grinding.

Mechanical testing was carried out using closed loop, computer assisted servohydraulic or electromechanical systems with a load capacity of 100 kN. The specimen grips were specially developed and allow a precise axial loading in both tension and compression. To achieve low levels of specimen bending during a test series, constant accurate manufacturing and centric clamping of specimens have to be ensured. For the determination of superimposed bending, a cylindrical reference specimen with three sets of four strain gauges placed symmetrically along the specimen gauge length was loaded to a maximum of 0.1% axial strain in tension and compression (7). According to the french standard NF A 03-403 1990, a maximum of 10% bending strain at this point can be accepted. In round robin experiments we further observe the formation of surface cracks on the whole surface of the gauge length after LCF-testing at high temperatures for a large variety of materials, even for those with a high crack sensitivity (8). This is consistent with the low levels of specimen bending measured at room temperature. All testing systems are equipped with three-zone furnaces in order to achieve temperature differences less than 3 K along the gauge length up to 1150°C during testing. The effective gauge length of the extensometers was 21 mm.

The tests were carried out with uncoated specimens in air under total strain control with a triangular waveform ($R_\varepsilon = -1$). The absolute value of the strain rate was in most experiments 10^{-3} s^{-1}, but some results for 10^{-4} s^{-1} and 10^{-5} s^{-1} are also available. Hold periods of 300 s were introduced at either the maximum or the minimum strain level and are represented as t_t and t_c respectively. For each hysteresis loop the mean stress σ_m was defined as $\sigma_m = \frac{1}{2}(\sigma_{max} + abs(\sigma_{min}))$ and the total stress range as $\Delta\sigma = 2\,\sigma_m$. The specimen lifetime, N_A, was determined through a macroscopic crack initiation criterion from the diagram total stress range *versus* cycle number, N (7,8).

Mechanical behaviour

Figure 2 shows the dependence of the cycle number for crack initiation, N_A, on the total strain range, $\Delta\epsilon_t$, for SRR99 at 980°C. This log-log-diagramm shows the results of LCF tests without hold periods (▲), with hold periods of t_t = 300 s at the maximum tensile strain (□) or with hold periods of t_c = 300 s at the maximum compressive strain (⊠). For the sake of simplicity, the results for these three loading types were connected by straigth lines, which do not involve any theoretical consideration. The relatively narrow scatter in N_A observed for tests without hold periods can be exemplified by the results of seven tests with $\Delta\epsilon_t$ = 0.7%. The angle χ for these specimens varied between 2.5° and 5.5°. Three of them were ground in longitudinal direction, the other four as usual in circumferential direction.

The introduction of a hold period in the compressive phase led in comparison to the tests without hold periods to a drastic reduction in N_A up to one order of magnitude in the range investigated. On the other hand, the introduction of a hold period in the tensile phase led to a moderate reduction in N_A for large values of $\Delta\epsilon_t$, whereas for lower values of the total strain range an increase in lifetime was observed.

The mean stress during tests without hold periods was less than 1% of the total stress range. The introduction of hold periods in the compressive phase led to a shift of the hysteresis loop in the tensile stress region, so that the mean stress reached values of about 15% of the total stress range after few cycles and kept approximately constant up to N_A. The inverse tendency was observed for tests with a hold period in the tensile phase. The total stress ranges for tests with the same value of $\Delta\epsilon_t$ was nearly independent of the specific cycle waveform.

The LCF-behaviour of CMSX-6 at 980°C is shown in Figure 3. There is an evident similarity to the response of SRR99 under the same conditions, which includes all other observations made above.

Figure 4 shows the dependence of N_A on $\Delta\epsilon_t$ for SC 16 at 950°C. The LCF tests were carried out in air with strain rates of 10^{-3} s^{-1}, 10^{-4} s^{-1} and 10^{-5} s^{-1}. There is no clear evidence of a strain rate influence on the lifetime of the specimens. The effect of hold periods on the LCF-behaviour of SC 16 is currently being investigated and will be presented elsewhere.

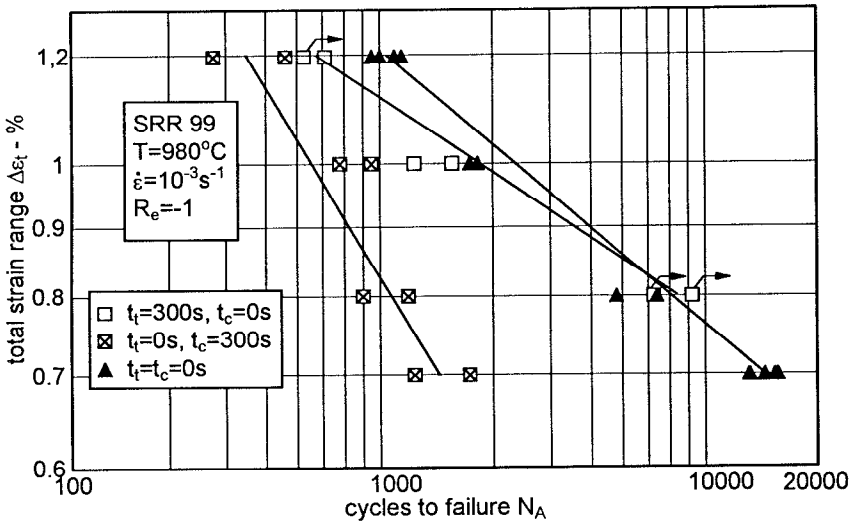

Figure 2: SRR99
LCF-tests at 980°C

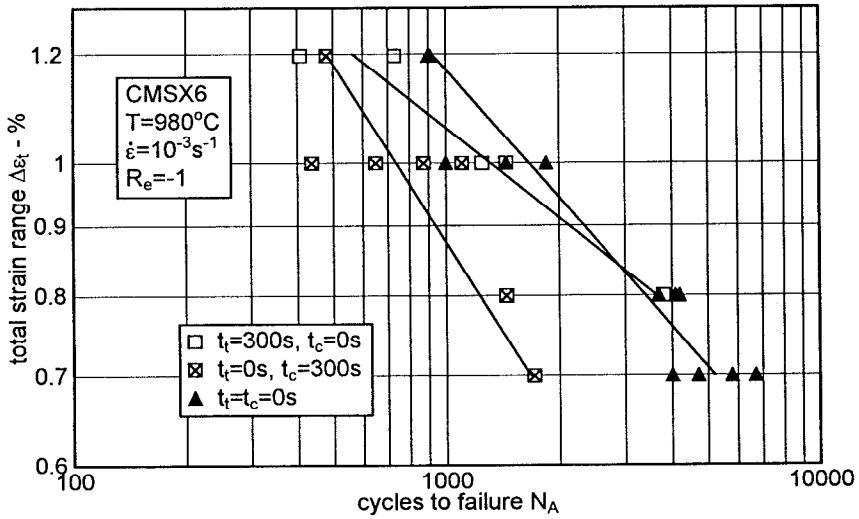

Figure 3: CMSX-6
LCF-tests at 980°C

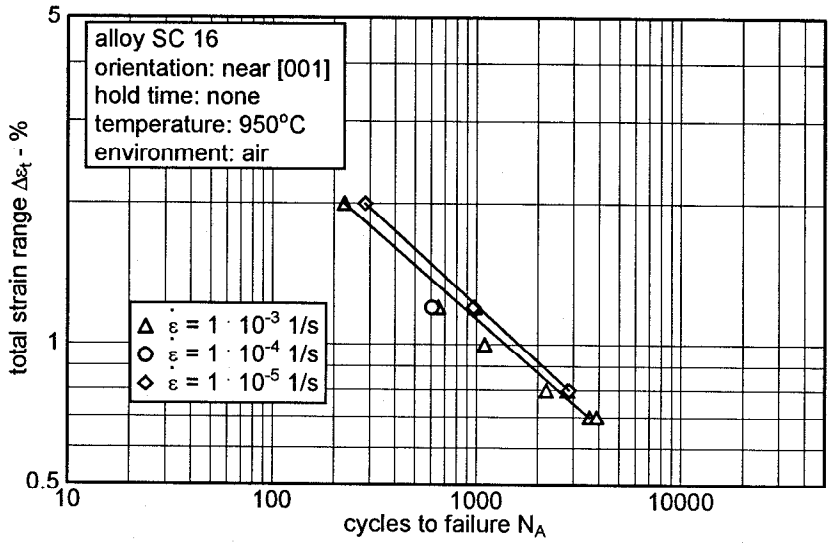

Figure 4: SC 16
LCF-tests at 950°C

Microstructural evolution

Figure 5 shows the microstructural evolution for SRR99 under LCF loading without hold periods. There is a slight tendency of the γ'-particles to interconnect and form plates parallel to the specimen axis. These changes are accompanied by an almost linear reduction in $\Delta\sigma$ with increasing N. The sharp softening observed at the beginning of the tests, which was completed after few cycles, can not be associated with any change in the γ/γ'-microstructure. On the other hand, the large reduction in $\Delta\sigma$ after N_A is due to the growth of the main crack and will be discussed below. Since the presence of a large crack leads to the unloading of large parts of the specimen, we do not observe any signifcant changes in the γ/γ'-microstructure between crack initiation and final fracture, as can be seen in Figure 5 by comparing the two SEM micrographs on the right side.

The changes in the γ/γ'-microstructure of SRR99 under LCF loading with $\Delta\epsilon_t$ = 1.2% are presented in Figure 6 . The upper curve shows for a strain rate of 10^{-3} s^{-1} the same evolution as reported above for $\Delta\epsilon_t$ = 0.7%. On the other hand, the much longer tests with a strain rate of 10^{-5} s^{-1} show a much more pronounced softening with increasing N and drastic microstructural changes. After few cycles with the lower value of the strain rate, we observed (left SEM micrograph) nearly the same γ/γ'-microstructure as after the test with 10^{-3} s^{-1}. The duration of these both tests was nearly the same. The pronounced softening observed for larger N values is associated with a notable coarsening of the γ'-particles, which assume the form of folded plates, the segments of which lie on (111) planes. This unusual configuration was confirmed by preparing two longitudinal sections perpendicular to each other and a transversal section for SEM and by preparing thin foils from a tranversal section for TEM, Figure 7.

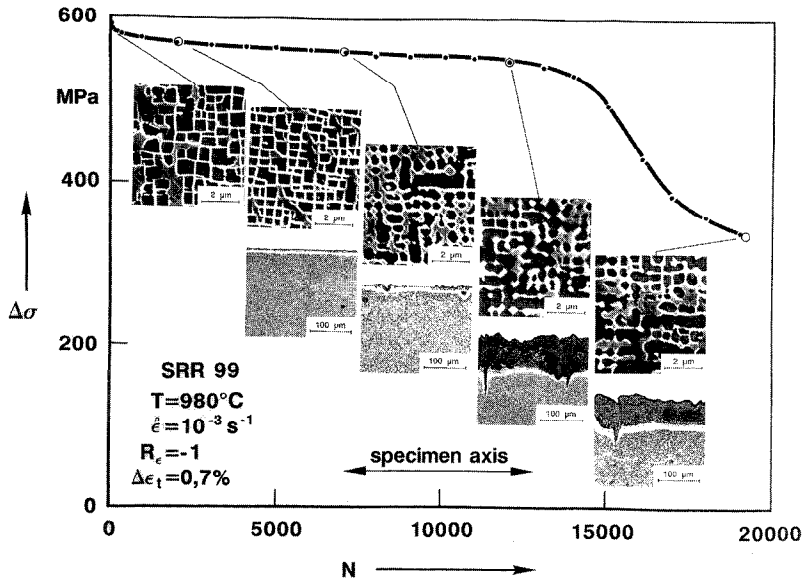

Figure 5: SRR99
Microstructural evolution
during a LCF-test

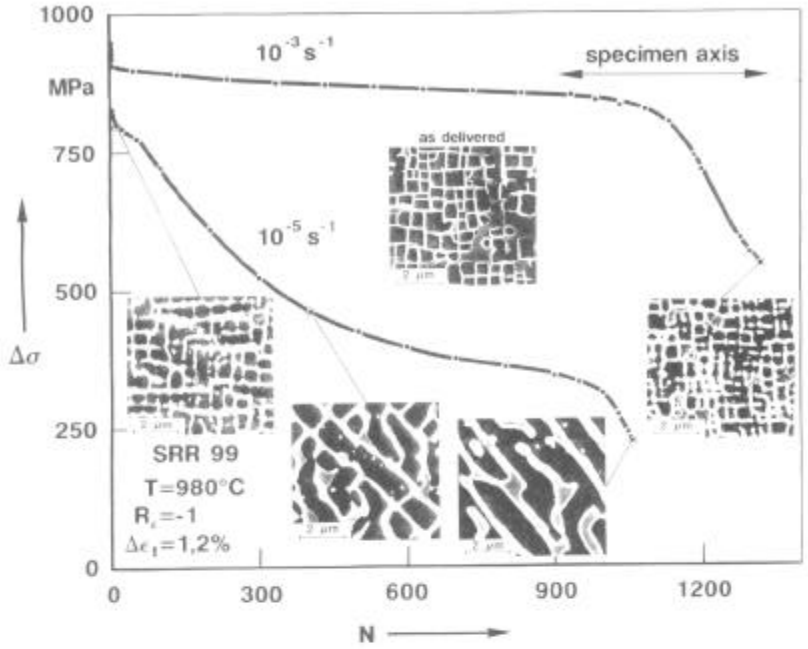

Figure 6: SRR99
Microstructural evolution during LCF-tests with different strain rates

The introduction of hold periods in the tensile phase leads to the formation of γ-plates in a γ'-matrix oriented perpendicular to the specimen axis, Figure 8a, whereas hold periods in the compressive phase lead to γ-plates parallel to the specimen axis, Figure 8b.

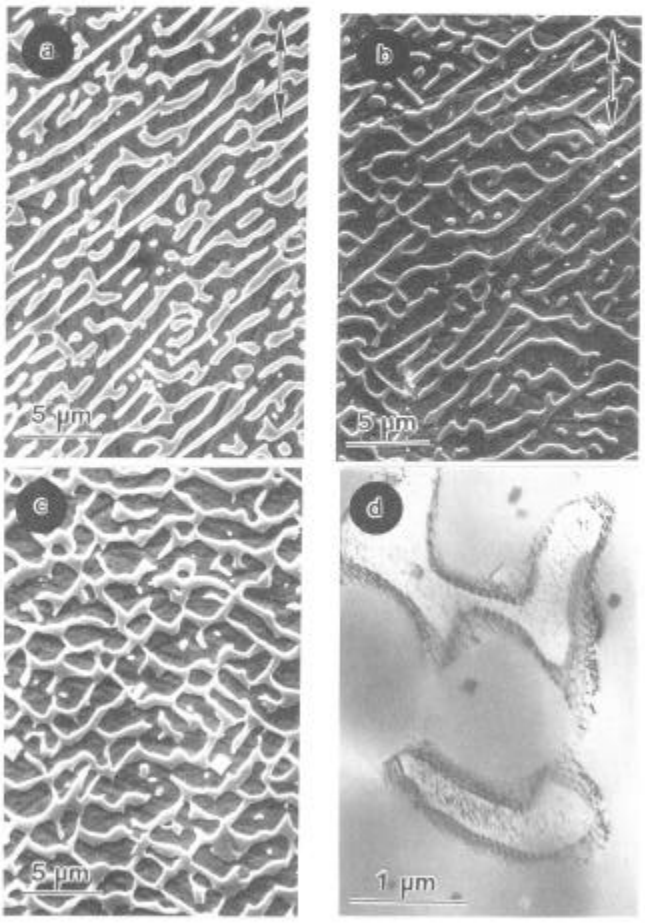

Figure 7: SRR99
Microstructure after a LCF-test at 980°C with $\Delta\varepsilon_t$ = 1.2%, R_ε = -1 and $\dot{\bar{\varepsilon}}$ = 10^{-5} s^{-1}
a,b) longitudinal section (SEM); c) tranversal section (SEM); d) tranversal section (TEM)

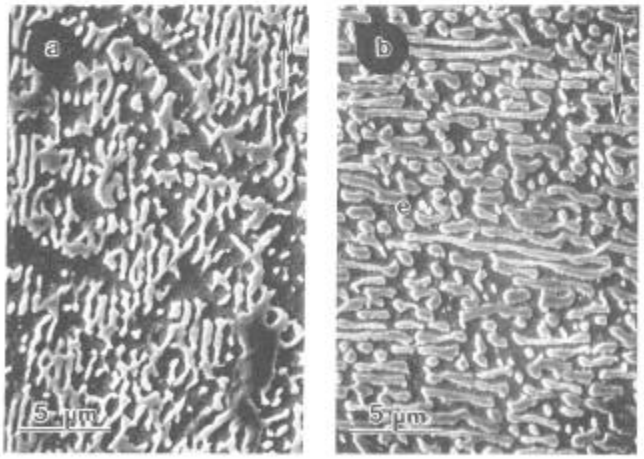

Figure 8: SRR99
Microstructure after LCF-tests at 980°C with $\Delta\varepsilon_t$ = 1.0%, R_ε = -1, $\dot{\bar{\varepsilon}}$ = 10^{-3} s^{-1} and hold periods of 300 s in the:
a) compressive phase; b) tensile phase

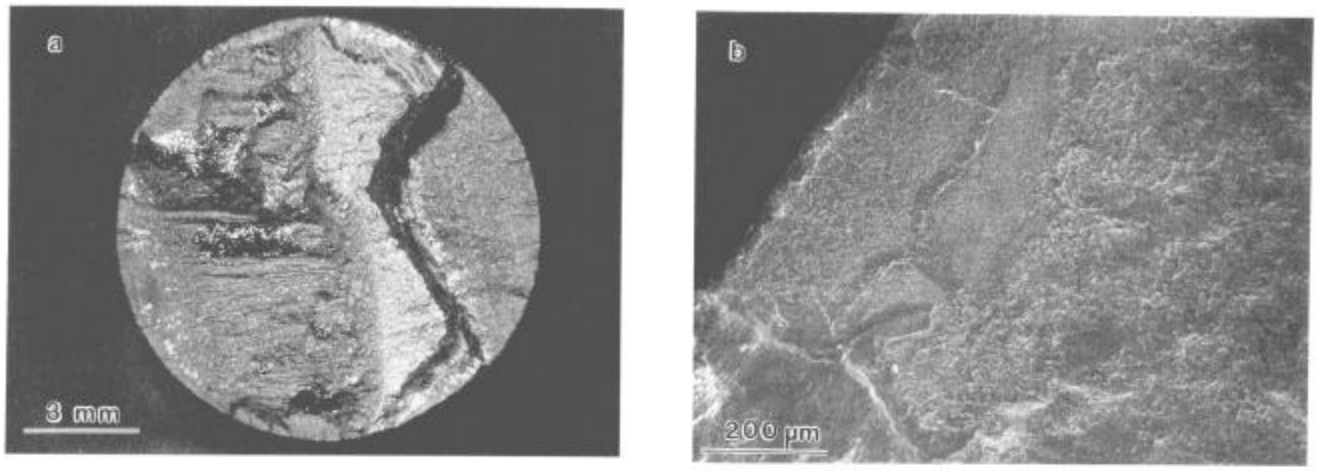

Figure 9: SRR99
Fracture surface after a LCF-test at 980°C with $\Delta\varepsilon_t = 0.7\%$, $R_\varepsilon = -1$ and $\dot{\varepsilon} = 10^{-3}\ s^{-1}$
a) overview; b) surface crack (SEM)

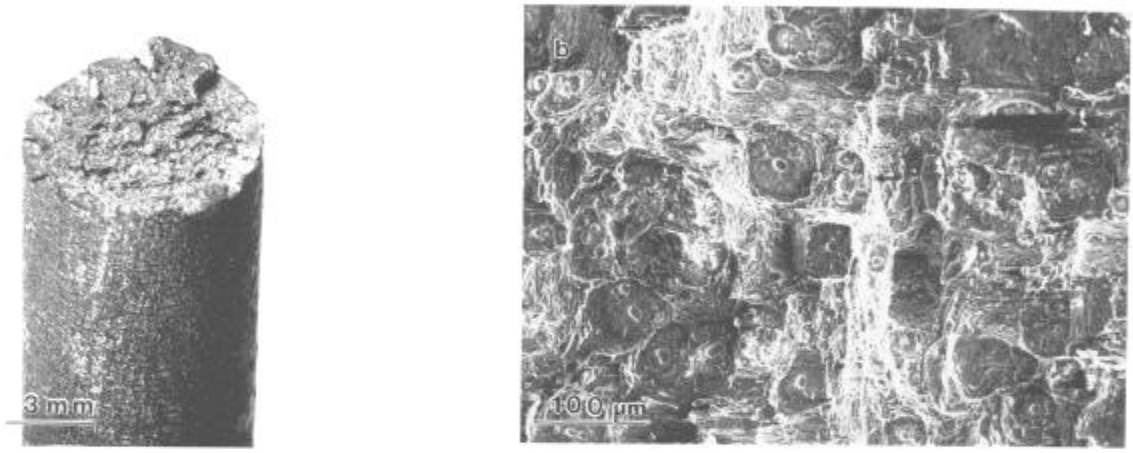

Figure 10: SRR99
Fracture surface after a LCF-test at 980°C with $\Delta\varepsilon_t = 0.7\%$, $R_\varepsilon = -1$ and $\dot{\varepsilon} = 10^{-3}\ s^{-1}$ and hold periods of 300 s in the compressive phase:
a) overview; b) fatigue lines in the inclined surface (SEM)

Figure 11: SRR99
Fracture surface after a LCF-test at 980°C with $\Delta\varepsilon_t = 0.7\%$, $R_\varepsilon = -1$ and $\dot{\varepsilon} = 10^{-3}\ s^{-1}$ and hold periods of 300 s in the tensile phase:
a) overview; b) detail of the fracture surface, the square regions are typical for creep fracture (SEM)

Fracture mechanisms

The light micrographs in Figure 5 show the evolution of the damage mechanism under LCF loading without hold times. The formation of a complex oxide layer (mainly containing nickel and aluminium) after few cycles depletes a surface near region of Al, resulting in a γ'-free layer. Both layers grow steadily with increasing value of N, but at some preferential sites distributed homogeneously over the specimen surface, the formation of nickel oxide speeds up. At these sites we observe protusions on the surface, under which small cracks perpendicular to the specimen axis are hidden. In the metallographical specimens these cracks are clearly identifiable as "spikes" running ahead of the normal corrosion front. These surface cracks grow laterally and may link to form the main crack, which grows more rapidly into the specimen. This point corresponds to the failure criterion defined above for N_A. The resulting fracture surface is nearly plane and perpendicular to the specimen axis, but the ligament usually shows a shear component, Figure 9a. Near to the specimen border, the fracture surface deflects and sets free some small surface cracks, which show a "thumb nail" shape, Figure 9b.

The initial stages of damage under LCF loading with hold periods are identical. However, the behaviour of the surface cracks after being formed changes radically in these cases. With hold periods in the compressive phase, the surface cracks stop growing laterally at some point. Sharp inclined cracks are generated at their extremities, some of them grow more rapidly and determine the rupture. The fracture surface consists of two or more inclined surfaces which are nearly ((111)) oriented, Figure 10a. The steps observed on these surfaces suggest clearly the cyclic nature of the growth these cracks, Figure 10b.

With hold periods in the tensile phase, surface cracks do form but become inactive. Instead of them, cracks originating from bulk pores grow and become predominant. The surface fracture is nearly plane and perpendicular to the specimen axis, Figure 11a, but it shows typical features of creep fracture in these alloys, Figure 11b. In the two other loading types we did not observe any damage at the bulk pores.

Discussion

The evolution of the γ/γ'-microstructure in single crystal superalloys is classically considered to be a diffusional process which depends strongly on the misfit between the γ and the γ' phases as well as on the applied stress (9). Our results concerning the evolution of the γ/γ'-microstructure in SRR99 and CMSX-6 under LCF loading with hold periods are in accordance with this approach. Both alloys have a negative misfit and show platelets perpendicular to the specimen axis when hold periods are introduced in the tensile phase, since in this case the specimen was submitted the far most long time to a tensile stress. *Mutatis mutandis* they present platelets parallel to the specimen axis when the predominant stress is compressive. These structures show significant long range internal stresses, which could be associated to the asymmetry observed in the σ-ϵ-loops.

However, this classical approach does not consider the strain component. Since the dislocation structure may influence diffusional processes, strain might play a significant rôle. In fact, LCF tests of long duration generate platelet structures which can not be explained by a stress argument alone. The observed softening during those tests seems to be connected to the formation of matrix channels which allow the reversible glide of dislocations. In this case, the long range internal stresses should not be very high. This would be consistent with the observed symmetrical shape of the σ-ϵ-loops.

When considering the LCF behaviour of superalloys, hold periods in the compressive phase are more damaging than those in the tensile phase, which is usually associated with the high mean stress levels resulting from assymetric loading (2). The single crystal superalloys SRR99 and CMSX-6 show at 980°C the same behaviour as reported in the literature. However, the shift in the mean stress seems to be connected with the changes observed in the γ/γ'-microstructure and the consequent formation of internal stresses. The radically different fracture mechanisms observed under these loading types are currently being investigated in more detail. We expect to derive from these investigations more concrete clues to the behaviour of superalloys under cyclic loading.

Acknowledgements

This work was partially supported by the *Bundesministerium für Bildung und Forschung* (03 M3038 D), by the *Deutsche Forschungsgemeinschaft* (Sfb 339, B7 and C1) and by the European Community (BriteEuram BRE2-CT92-0176). We are grateful for the experimental support given by Bärbel Bogel, Uwe Chrzanowski, Klaus Naseband, Wolfgang Wedell and Jörg Wuttke.

References

1. Josef Ziebs, Jürgen Meersmann, Hans-Joachim Kühn, Norbert Hülsmann and Jürgen Olschewski, "Multiaxial thermomechanical behaviour of IN 738 LC,", in: Proceedings of the 4th International Conference on Biaxial/Multiaxial Fatigue, vol. 2, (European Structural Integrity Society, 1994), 247-259.

2. W.J. Plumbridge and E.G. Ellison, "Low-cycle-fatigue behaviour of superalloy blade materials at elevated temperature," Materials Science and Technology 3(9)(1987), 706-715.

3. Alfred Donner, "Gerichtete Erstarrung - ein bauteilgerechtes Herstellverfahren für Turbinenschaufeln," Metall, 42(2)(1988), 128-132.

4. Pedro D. Portella, Konrad Breitkreutz and Veronica Bierwagen, "Quantitative Analyse von Gefügeänderungen in einkristallinen Superlegierungen," in: *Sonderbände der Praktischen Metallographie*, vol. 23, ed. W.-U. Kopp *et al.* (Munich, BY: Carl Hanser Verlag, 1992), 93-106.

5. Uwe Chrzanowski, Hellmuth Klingelhöffer, Pedro D. Portella and Konrad Breitkreutz, "Gefügeveränderungen der einkristallinen Nickel-Basis-Superlegierung SC 16 bei Kriechbeanspruchung und deren quantitative Auswertung," in: *Sonderbände der Praktischen Metallographie*, vol. 27, ed. M. Kurz and M. Pohl (Oberursel, HS: DGM-Informationsges. mbH, 1995), 255-258.

6. M.J. Goulette, P.D. Spilling and R.P. Arthey, "Cost effective single crystals," in: Proceedings of the 5th International Symposium Superalloys, ed. M. Gell *et al.* (Warrendale, PA: The Minerals, Metals & Materials Society, 1984), 167-176.

7. Klaus Naseband, Siegfried Ledworuski, Hans-Joachim Kühn and Holger Frenz, "High-temperature low-cycle-fatigue testing," in: Proceedings of the 6th International Fatigue Congress 1996 (London: Elsevier Applied Science, in press).

8. Klaus Naseband and Rolf Helms, "Low-cycle fatigue testing programme," (Report BCR contract 2119/1/4/269/85/3, BAM, 1989).

9. André Pineau, "Influence of uniaxial stress on the morphology of coherent precipitates during coarsening - elastic energy considerations," Acta metall. 24 (1976), 559-564.